Food & Function

Accepted Manuscript

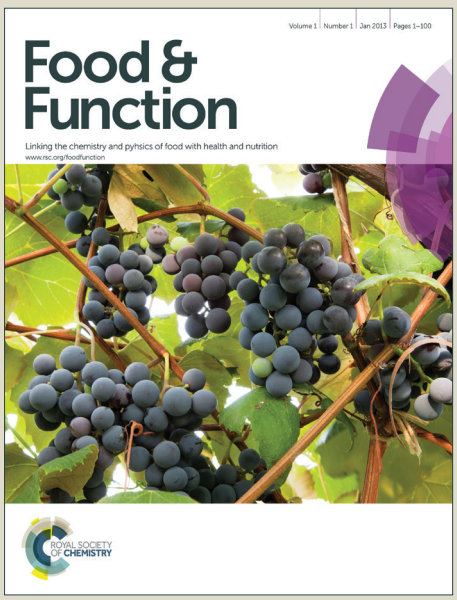

This is an *Accepted Manuscript*, which has been through the Royal Society of Chemistry peer review process and has been accepted for publication.

Accepted Manuscripts are published online shortly after acceptance, before technical editing, formatting and proof reading. Using this free service, authors can make their results available to the community, in citable form, before we publish the edited article. We will replace this *Accepted Manuscript* with the edited and formatted *Advance Article* as soon as it is available.

You can find more information about *Accepted Manuscripts* in the Information for Authors.

Please note that technical editing may introduce minor changes to the text and/or graphics, which may alter content. The journal's standard Terms & Conditions and the Ethical guidelines still apply. In no event shall the Royal Society of Chemistry be held responsible for any errors or omissions in this *Accepted Manuscript* or any consequences arising from the use of any information it contains.

ROYAL SOCIETY OF CHEMISTRY

www.rsc.org/foodfunction

Graphic for Table of Contents

The biological activities of azo colorant may significantly be influenced by the biointeraction of ligand to protein in the human body.

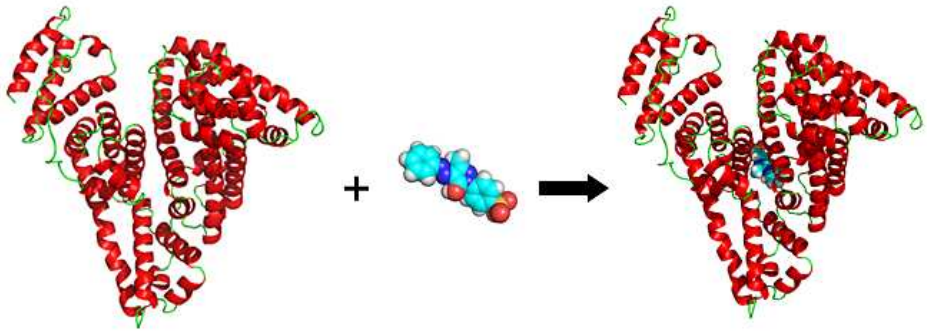

Evaluation of the Biointeraction of Colorant Flavazin to Human Serum Albumin: Insights from Multiple Spectroscopic, *in Silico* Docking and Molecular Dynamics Simulation

Wei Peng,[†ab] Fei Ding,*[†bc] Yu-Ting Jiang,[d] Ying Sun[e] and Yu-Kui Peng*[a]

[a] *College of Food Science & Engineering, Northwest A&F University, Yangling 712100, China*

[b] *Department of Chemistry, China Agricultural University, Beijing 100193, China*

[c] *Department of Biological Engineering, Massachusetts Institute of Technology, Cambridge, MA 02139, United States*

[d] *Department of Chemistry, University of Ottawa, 10 Marie Curie, Ottawa, ON K1N 6N5, Canada*

[e] *College of Resources and Environmental Sciences, China Agricultural University, Beijing 100193, China*

[†]These authors contributed equally to this work.

*Corresponding author
Phone/fax: +86-29-87092367
E-mail: alexf.ting@gmail.com, feiding@cau.edu.cn (F. Ding); pyk2009@nwsuaf.edu.cn (Y.-K. Peng).

ABSTRACT

Azo compounds are the largest chemical class of agents frequently used as colorants in a variety of consumer goods and farm produce; therefore they may become a hazard to public health, because numerous azo compounds and their metabolites are proven to be carcinogens and mutagens. Herein several qualitative and quantitative analytical techniques, based on steady state and time-resolved fluorescence, circular dichroism (CD), computer-aided molecular docking as well as molecular dynamics simulation was employed to ascertain the molecular recognition between the principal vector of ligands in human plasma, albumin and a model azo compound flavazin. The results show that the albumin spatial structure was changed in the presence of flavazin with a decrease of α-helix suggesting protein partially destabilization/self-regulation, as derived from steady state fluorescence, far-UV CD and detailed analyses of three-dimensional fluorescence spectra. Time-resolved fluorescence further evinced the recognition mechanism belongs to the albumin-flavazin adduct formation with an association intensity of 10^4 M^{-1}, and the driving forces were found to be chiefly π-π, hydrophobic interactions and hydrogen bonds. Intuitively, the accurate binding domain of flavazin in protein has been defined from molecular docking, subdomain IIA (Sudlow's site I) was designated to retain high-affinity for ligand flavazin, this corroborates the competitive ligands displacement, hydrophobic 8-anilino-1-naphthalenesulfonic acid probe and chemical unfolding of protein results laying the flavazin at warfarin-azapropazone site. Based

on molecular dynamics simulation, we can be said with certainty that the results of molecular docking are credible, and the key amino acid residues participating in the molecular recognition of flavazin by protein are clearly Trp-214, Arg-222 and Lys-436. The outcomes presented here will help to further comprehend the molecular recognition of azo compound by protein and the possible toxicological profiles of other compounds which have analogous configuration with azo chemicals.

KEYWORDS: *molecular recognition, albumin, azo compound, circular dichroism, molecular dynamics simulation*

INTRODUCTION

Colorants create the world more gorgeous through colored substances, but then they denote a severe pollution conundrum for the environment.[1] From the available literature it can be appraised that the total dye utilization of the textile industry worldwide is more than 10^7 kg per year, and under usual manufacturing and dying procedure, up to 50% of the dyes are lost after the dying process and about 10～15% of them are discharged in the effluents and ultimately expelled into the environment.[2] The release of those colored wastewater in the environment is a huge fount of non-aesthetic pollution because the presence of small quantities of dye (below 1 ppm) is obviously visible.[3]

On the basis of the Color Index, which are managed by the Society of Dyers and Colorists and American Association of Textile Chemists and Colorists, now more than 10,000 various types of colorants are synthesized and useable in the world, among these colorants, azo compounds compose the largest and most versatile class of colorants with exceed 65% of the colorants being currently used.[4] Azo dyes have a coloring effect involving one or more azo group (−N=N−) in their molecular structure, and are massively used for coloring a variety of consumer goods, such as textiles, paper, food, drink, leather, drug, cosmetics, ink, clothes and toys, owing to their variety of color shades, superior fastness, high stability, brilliant colors, and ease of application.[5,6] Because azo dyes are heavily applied, as a matter of fact, azo colorants always pervades our daily life, they must be present in greatly or relatively

high concentrations in our farm produce, commodities or water originating from manufacturing industry or nature.

Regrettably, epidemiologic and histopathologic studies have clearly shown azo dyes may be highly toxic and potentially mutagenic and carcinogenic for experimental animals and humans, and their degradation products such as aromatic amines and its derivatives were also known to be carcinogenic.[7-10] For examples, the azo dye amaranth has been proved to be carcinogenic for rats,[11] but this dye was extensively employed as a food colorant in many countries such as the European Union.[12] In a report prepared by Amin et al.,[13] two food azo colorants, tartrazine and carmoisine have been fed orally young male (*Rattus Norvegicus*) Albino rats in two doses, one low and the other high dose for 30 days. They demonstrated evidently that the boost of transaminase activities and the reduced cholesterol level in blood serum may probably be owing to organ damage especially in liver, kidney and heart; and the raised levels of aspartate transaminase and alanine transaminase displays injury of both hepatic cellular and mitochondrial membranes in food azo colorants administered rats. In 2012, Yadav et al.[14] performed *in vitro* studies on immunotoxic concealed of a synthesized azo compound Orange II in splenocytes of female BALB/c mice and Swiss mice. They considered that Orange II was notably poisonous to splenocytes and the non-cytotoxic potion was found to be 50 μg mL^{-1}, Orange II has a total suppressive effect on the mitogen activated release of cytokines included in the stimulation of cellular, humoral or inherent immunity; therefore they inferred that chronic contact of Orange II to human may harm the capability of immune system to

battle causative agents efficaciously.

It is noteworthy that the azo colorants have numerous structural variety that are exceedingly stable under exposure to light and washing, and resistant to aerobic biodegradation by bacteria, thereby azo compounds have attracted crucial attention from the toxicological and environmental points of view, particularly in light of the current increase in their applications.[15,16] Consequently, the existence of different azo colorants in the environment (i.e. ground and surface water) and in the final industrial commodities may represent a huge risk for human health. Probably, these azo compounds will be produced negative effects on human health if they enter the body, regardless of direct or indirect routes. These are some persuasive evidences certifies the toxicological action of various chemicals for human does not come predominantly from acute toxicity; however, it is mainly because of the long term and chronic accumulation of these compounds in the human body. Ideally, almost any ligands, either pharmacological or toxicological activities, would ultimately interact with several important biomacromolecules such as enzymes, nucleic acids and proteins through noncovalent bonds when they present in different organs or organelles. The strength of these noncovalent interactions, together with the conformational changes of biological macromolecules, will clinically assume disparate symptoms of many illnesses. For that reason the discussion of concrete information regarding the noncovalent interactions between various chemicals and biopolymers will assist us realize the pathogenesis of many diseases at the molecular scale, and successfully development of homologous treatments or pharmaceuticals. According to the today's

stylish perception, the molecular recognition of different compounds by key blood components is able to affect their biological activity and biomacromolecule function; on this account, the analysis of their binding to plasma proteins symbolizes an extremely important tool to gain toxicological information of how azo compounds impacts on human health.[17,18]

The outstanding plasma and tissue protein which is habitually responsible for the nonspecific binding of most ligands is albumin (Fig. 1). It is the most copious plasma protein with a molecular weight of 66.5 kDa, and exhibits an average half-life of 19 days. Despite its large molecular mass, albumin is not exclusively reserved in the plasma but is also dispersed extravascularly.[19] The unique physiological function of albumin account for the principal role it can play in both the efficacy and rate of delivery of ligands, generally through the formation of noncovalent complex, and influencing the absorption, distribution, metabolism, excretion and toxicity of diverse endogenous and exogenous substances.[20,21] It is consequently proper to contemplate the function of albumin in influencing ligand binding, pharmacokinetics or toxicokinetics and ultimately their biological activity. With this background, the goal of the present work was to assess the molecular recognition process as well as the spatial structure of the complexes formed between albumin and the model azo compound flavazin (structure shown in Fig. 2) by employing steady state fluorescence, circular dichroism (CD) and three-dimensional fluorescence. Specifically, the association affinity and binding patch of flavazin in albumin was characterized by time-resolved fluorescence, site-specific ligands, hydrophobic

8-anilino-1-naphthalenesulfonic acid (ANS) displacement along with protein denaturation with guanidine hydrochloride (GuHCl). Finally, these experimental observations were further interpreted on the basis of molecular docking and molecular dynamics simulation executed for the protein-ligand system, in order to receive comprehensive interpretation of the albumin-azo colorant complex as well as in understanding the physiological and toxicokinetic clues of the azo compound.

Fig. 1 here about

Fig. 2 here about

EXPERIMENTAL

Materials. Albumin from human serum (A3782, lyophilized powder, fatty acid free, globulin free, ≥ 99%), flavazin (F8879) and 8-anilino-1-naphthalenesulfonic acid (A1028, ≥ 97%) were purchased from Sigma-Aldrich (St. Louis, MO, USA) and used without further purification, and deionized water was generated by a Milli-Q Ultrapure Water Purification Systems from Millipore (Billerica, MA, USA). Tris (0.2 M)-HCl (0.1 M) buffer of pH＝7.4, with an ionic strength 0.1 in the presence of NaCl, and the pH was checked with an Orion Star A211 pH Benchtop Meter (Thermo Scientific, Waltham, MA, USA). Dilutions of the albumin stock solution (10 μM) in Tris-HCl buffer were prepared immediately before use, and the concentration of albumin was measured spectrophotometrically using $E_{1\ \mathrm{cm}}^{1\%} = 5.3$.[22] All other reagents employed were of analytical grade and received from Sigma-Aldrich. To

remove any undissolved matter, all samples were filtered through a 0.22 μm Millex-GV Filter (Millipore, Billerica, MA, USA).

Fluorescence Emission. Steady state fluorescence was obtained with a 1.0 cm path length quartz cell using a F-7000 spectrofluorimeter (Hitachi, Japan) equipped with a thermostatic bath. The excitation and emission slits were set at 5.0 nm each, intrinsic fluorescence was carried out by exciting the continuously stirred protein solution at 295 nm to favor tryptophan (Trp) excitation, and the emission spectra were read in the wavelength range of 300-450 nm at a scanning speed of 240 nm min^{-1}. The reference sample consisting of the Tris-HCl buffer of flavazin in corresponding concentrations was subtracted from all fluorescence measurements.

CD Spectra. Far-UV CD spectra were collected with a Jasco-815 spectropolarimeter (Jasco, Japan) equipped with a microcomputer, the apparatus was sufficiently purged with 99.9% dry nitrogen gas before starting the instrument and then it was calibrate with d-10-camphorsulfonic acid. All the CD spectra were got at 298 K with a PFD-425S Peltier temperature controller attached to a water bath with an accuracy of ± 0.1 ^{o}C. Each spectrum was performed with use of a precision quartz cuvette of 1.0 cm path length and taken at wavelengths between 200 and 260 nm range that provides a signal extremely sensitive to small secondary conformational distortions. Every determination was the average of five successive scans encoded with 0.1 nm step resolution and recorded at a speed of 50 nm min^{-1} and response time of 1 s. All observed CD data were baseline subtracted for buffer and the estimation of the secondary structure elements was obtained by exploiting Jasco Spectra Manager II,

177 which computes the different designations of secondary structures by comparison
178 with CD spectra, determined from distinct proteins for which high-quality X-ray
179 diffraction data are available.

180 **Three-dimensional Fluorescence.** The emission wavelength was scanned
181 between 200 and 500 nm, the initial excitation wavelength was set to 200 nm with
182 increment of 10 nm, the number of scanning curves was 16, and the other scanning
183 parameters were identical to the fluorescence emission above.

184 **Time-resolved Fluorescence.** Time-resolved fluorescence was examined with a
185 FLS920 spectrometer (Edinburgh Instruments, UK), using the time-correlated single
186 photon counting system with a hydrogen flash lamp excitation source, in air
187 equilibrated solution at an ambient temperature. The excitation wavelength was 295
188 nm and the number of counts gathered in the channel of maximum intensity was
189 4,000. The instrument response function (IRF) was gauged exploiting Ludox to
190 scatter light at the excitation wavelength. The data were analyzed with a nonlinear
191 least-squares iterative method utilizing the Fluorescence Analysis Software
192 Technology, which is a sophisticated software package designed by Edinburgh
193 Photonics for the analysis of fluorescence and phosphorescence decay kinetics, IRF
194 was deconvoluted from the experimental data, and the resolution limit after
195 deconvolution was 0.2 ns. The value of χ^2 (0.9～1.2), the Durbin-Watson parameter
196 (greater than 1.7), as well as a visual inspection of the residuals were used to assess
197 how well the calculated decay fit the data. Average fluorescence lifetime (τ) for
198 multiexponential function fittings were from the following relation:[23]

$$I(t) = \sum_i A_i e^{\frac{-t}{\tau_i}} \quad (1)$$

where τ_i are fluorescence lifetimes and A_i are their relative amplitudes, with i variable from 1 to 2.

Site-specific Ligand. Binding location studies between albumin and flavazin in the presence of four typical site markers (warfarin, diazepam, digitoxin and hemin) were executed using the fluorescence titration approach. The concentration of albumin and site markers were held in equimolar (1.0 μM), then flavazin was added to the albumin-site markers mixtures. An excitation wavelength of 295 nm was chosen and the fluorescence emission wavelength was acquired from 300 to 450 nm.

Hydrophobic ANS Displacement. In the first series of experiments, albumin concentration was kept fixed at 1.0 μM, and flavazin/ANS concentration was varied from 1.0 to 7.0 μM, albumin fluorescence was gained (λ_{ex}＝295 nm, λ_{em}＝350 nm). In the second series of experiments, flavazin was added to solutions of albumin and ANS held in equimolar concentration (1.0 μM), and the concentration of flavazin was also varied from 1.0 to 7.0 μM, the fluorescence of ANS was recorded (λ_{ex}＝370 nm, λ_{em}＝465 nm).

Molecular Docking. Molecular docking of the albumin-flavazin complex was operated on SGI Fuel Visual Workstation. The crystal structure of albumin (entry codes 1AO6), determined at a resolution 2.5 Å,[24] was retrieved from the Brookhaven Protein Data Bank (http://www.rcsb.org/pdb). After being imported in the program Sybyl Version 7.3 (http://tripos.com),[25] albumin structure was carefully checked for atom and bond type correctness assignment. Hydrogen atoms were computationally

added using the Sybyl Biopolymer and Build/Edit menus. To avoid negative acid/acid interactions and repulsive steric clashes, added hydrogen atoms were energy minimized with the Powell algorithm[26] with 0.05 kcal mol^{-1} energy gradient convergence criteria for 1500 cycles, this procedure does not change positions to heavy atoms, and the potential of the three-dimensional structure of albumin was assigned according to the AMBER force field with Kollman all-atom charges. The two-dimensional structure of flavazin was downloaded from PubChem (http://pubchem.ncbi.nlm.nih.gov), and the initial structure of the molecule was produced by Sybyl 7.3. The geometry of flavazin was subsequently optimized to minimal energy (tolerance of 0.5 kcal mol^{-1}) using the Tripos force field with Gasteiger-Hückel charges, and the lowest energy conformer was utilized for the docking analysis. The Surflex-Dock program which employs an automatic flexible docking algorithm was applied to analyze the possible conformation of the ligand that binds to albumin,[27] and the program PyMOL (http://www.pymol.org) was finally used for visualization of the molecular docking results.[28]

Molecular Dynamics Simulation. Molecular dynamics (MD) simulation of albumin-flavazin was performed using Gromacs program, version 4.5.5, with the Gromacs96 53a6 force field.[29,30] Initial conformations of albumin and flavazin were, respectively, taken from the original X-ray diffraction crystal structure that was solved at 2.5 Å resolution (entry codes 1AO6) and the optimal structure originated from molecular docking. The topologies of albumin were generated by Gromacs package directly, whereas flavazin by PRODRG2.5 server.[31] The simulation system was

243 solvated with a periodic cubic box (the volume is 7.335×6.155×8.119 nm^3) filled
244 with TIP3P water molecules and an approximate number (16) of sodium counterion to
245 neutralize the charge.[32] Totally, there are 51,226 crystallographic solvent molecules,
246 and the shortest distance between the complex and the edge of the box is set to 12 Å.
247 Simulations were carried out using the isothermal-isobaric (NPT) ensemble with an
248 isotropic pressure of 1 bar, and the temperature of the ligand, protein and solvent
249 (water and counterion) was separately coupled to an external bath held at 298 K,
250 using the Berendsen thermostat with 0.1 ps relaxation time.[33] The LINCS algorithm
251 was used to constrain bond lengths, and the long-range electrostatic interactions
252 beyond 10 Å were modeled using the Particle Mesh Ewald (PME) method with a grid
253 point density of 0.1 nm and an interpolation order of 4.[34,35] A cutoff of 12 Å was used
254 for van der Waals' interactions. The MD integration time step was 2.0 fs and covalent
255 bonds were not constrained, and the system configurations were saved every 2.0 ps.
256 To decrease the atomic collisions with each other, both gradient descent and conjugate
257 gradient algorithm were employed to optimize the whole system. First the solvated
258 starting structure was preceded by a 1,000-step gradient descent and then by
259 conjugate gradient energy minimization. Subsequently, 500 ps equilibration with
260 position restraints runs to remove possible unfavorable interactions between solute
261 and solvent, and after thorough equilibration, MD simulations were run for 10 ns.
262 Furthermore, the pure protein was also selected to execute a time period (10 ns) MD
263 simulations so as to compare with the first-rank molecular docking complex. The
264 results of MD simulations were finally displayed by Visual Molecular Dynamics

1.9.1,[36] and the program Discovery Studio Visualization 3.5 (Accelrys, San Diego, CA, USA) was utilized to show the images of the MD simulations.

Principles of Fluorescence Quenching. Fluorescence quenching refers to any process that decreases the fluorescence intensity of a sample. A variety of molecular interactions can result in quenching, such as excited state reactions, molecular rearrangements, energy transfer, ground state complex formation, and collisional quenching. Fluorescence quenching is described by the well-known Stern-Volmer equation[23]

$$\frac{F_0}{F} = 1 + k_q[Q] = 1 + K_{SV}[Q] \quad (2)$$

In this equation F_0 and F are the fluorescence intensities in the absence and presence of quencher, respectively, k_q is the bimolecular quenching constant, τ_0 is the lifetime of the fluorophore in the absence of quencher, [Q] is the concentration of quencher, and K_{SV} is the Stern-Volmer quenching constant. Therefore equation (2) was used to estimate K_{SV} by linear regression of a plot of F_0/F *versus* [Q].

Calculation of Recognition Ability. When ligand molecules bind independently to a set of equivalent sites on a macromolecule, the equilibrium between free and bound ligand molecules is given by the following relation:[37-39]

$$\log\frac{F_0 - F}{F} = \log K + n\log[Q] \quad (3)$$

$$\frac{F_0}{F} = \frac{K[Q_t]F_0}{F_0 - F} - nK[P_t] \quad (4)$$

In the two equations, F_0 and F are the fluorescence intensities in the absence and presence of ligand, respectively, K and n are the association constant and the number of binding sites, respectively; [Q] is the unbound concentration of ligand in the system,

however, it is difficult to determine the exact value for this parameter, so the term [Q] is generally replaced by [Q_t]; [Q_t] and [P_t] are the total concentration of ligand and biopolymer, respectively. Thus, a plot of $\log(F_0 - F)/F$ *against* $\log[Q]$ (equation (3)) or F_0/F *versus* $[Q_t]F_0/(F_0 - F)$ (equation (4)) can be used to calculate K and n. Moreover, the fluorescence intensities were corrected for absorption of the exciting light and reabsorption of the emitted light to decrease the inner filter effect by using the following relationship:[23]

$$F_{cor} = F_{obs} \times e^{\frac{A_{ex} + A_{em}}{2}} \quad (5)$$

where F_{cor} and F_{obs} are the fluorescence intensities corrected and observed, respectively, and A_{ex} and A_{em} are the absorption of the systems at the excitation and the emission wavelength, respectively. The fluorescence intensity utilized in this work is the corrected intensity.

RESULTS AND DISCUSSION

Steady State Fluorescence. As we know, tryptophan (Trp) is a comparatively sensitive fluorophore, when the intrinsic Trp residue fluorescence of a protein is keen to a ligand-protein occurrence, it could be applied as the discernible in the measurement of the recognition ability, binding mode and rate constant that characterize the process.[40,41] The association extent of albumin with flavazin were estimated by the measurement of intrinsic fluorescence of albumin Trp residue, and the steady state fluorescence for quenching of Trp in albumin with different amounts

of flavazin was shown in Fig. 3. Visibly, albumin indicated a maximum fluorescence peak at 350 nm following an excitation of 295 nm, and the addition of flavazin induced a regular decrease of the fluorescence intensity. Under the experimental conditions, flavazin displayed no fluorescence emission in the range 300～450 nm, which did not affect albumin intrinsic fluorescence. These observations demonstrated that there were reactions between albumin and flavazin, similar finding has been conveyed by Charbonneau et al.[42] for the recognition of cationic lipids by human serum albumin. Moreover, the maximum emission wavelength shifted from 350 nm to 354 nm, revealing the microenvironment around Trp residue was altered, and a higher hydrophilicity in the vicinity of Trp residue occurred.[43]

Fig. 3 here about

CD Spectra. Through the above it was obviously that there have been some fundamental conformational changes in protein structure. CD is, undeniably, a forceful analytical method to check the recognition of proteins with other ligands and to appraise the protein conformation in solution. In order to analyze the structural changes of albumin quantitatively, the far-UV CD spectra of albumin in the absence and presence of flavazin were monitored in Fig. S1 (Supporting Information), and secondary structure components computed based on raw CD data pooled in Table 1. The CD curves of albumin illustrated two negative peaks in the far-UV CD region at 208 nm and 222 nm, characteristic of α-helical structure of albumin. The logical explanation is that the negative bands between 208 and 209 nm and 222 and 223 nm are both contributed by $\pi \rightarrow \pi^*$ and $n \rightarrow \pi^*$ transition for the peptide bond of α-helix.[44]

Free albumin has 59.2% α-helix, 7.9% β-sheet, 13.5% turn and 19.4% random coil, after complex with flavazin, decrease of α-helix was seen from 59.2% free albumin to 48.6% (complex) while increase in β-sheet, turn and random coil from 7.9%, 13.5% and 19.4% free albumin to 9.4%, 16.1% and 25.9% (complex) at a molar ratio of albumin to dye of 1∶2. The reduction of α-helix with a growth in the β-sheet, turn and random coil evidencing flavazin bound with amino acid residues of the polypeptide chain and giving rise to the alteration of the albumin spatial structure, i.e. some degree of albumin destabilization upon flavazin conjugation.[45] The structural changes examined by far-UV CD spectra are in good agreement with steady state fluorescence (bathochromic effect) and are also in conformity with the three-dimensional fluorescence results below.

Table 1 here about

Three-dimensional Fluorescence. Extra proof of structural changes of albumin after complex with flavazin was represented by three-dimensional fluorescence (Fig. S2), and the commensurate parameters are merged in Table 2. This method, actually, guarantees that every probable excitation/emission coalition will be recorded by the spectrophotometer. It is evident to us from Fig. S2 that peak a ($\lambda_{ex}=\lambda_{em}$) is the Rayleigh scattering peak and peak b ($\lambda_{em}=2\lambda_{ex}$) is the second-order scattering peak. Apparently, peak 1 and peak 2 is the most significant three-dimensional fluorescence peak, and it mainly reflects the subtly structural quality of protein-flavazin complex; therefore the following analyses will be centered on the origin and property of the two peaks.

As set forth, proteins include three amino acid residues that contribute to their ultraviolet fluorescence which are habitually described by their abbreviations, i.e. Phe, Trp and Tyr. Although fluorescence emission of proteins is primarily dominated by Trp residue, which absorbs at the longest wavelength and shows the largest extinction coefficient, energy absorbed by Phe and Tyr residue is usually transferred to the Trp residues in the same protein.[23] When the excitation is fixed at 275 nm, Phe residue displays a structured emission with a maximum near 282 nm, the emission of Tyr residue in water arises at ~303 nm and is relatively insensitive to solvent polarity. The emission maximum of Trp residue in water occurs near 350 nm and is largely dependent on polarity and local environment, and the fluorescence intensity of Tyr is greater than the Trp residue.[46] Protein fluorescence is frequently excited at the absorption maximum near 280 nm accompanying an emission maximum at ~330 nm, and the emission wavelength and fluorescence intensity of protein is preserving between pure Tyr and Trp residue. We inferred that resonance energy transfer may occur from Phe to Tyr to Trp residue. In such situations, the donor is Phe and Tyr residue, and the receptor is Trp residue, leading to the decrease of Phe and Tyr fluorescence intensity following an excitation at 275 nm, and the growth of Trp fluorescence signal. With the fluorescence changes of these amino acid residues, and blue shifted Trp residues can transfer the excitation to longer wavelength Trp residue, it is safe to say that the fluorescence peak 1 originates from the overlay of the fluorescence features of Trp and Tyr residues.

Besides peak 1, there is another fluorescence peak 2 and the excitation wavelength

for this peak is 230 nm. We may reasonably conclude that peak 2 descends from the superposition of fluorescence of Phe, Trp and Tyr residues. Basically, the $\pi \rightarrow \pi^*$ transition of E_2 absorption band in aromatic ring structure can cause the fluorescence excitation at roughly 230 nm. However, the fluorescence emission peak of pure amino acids (Phe, Trp and Tyr) in aqueous solution does not correspond to the fluorescence emission peak of protein following the λ_{ex}＝230 nm and, as a result, this fact clearly denotes that the fluorescence emission of pure amino acids, that is Phe, Trp and Tyr would not simply superpose with an excitation of 230 nm. Chemically, proteins are unbranched polymers of amino acids linked head to tail, from carboxyl group to amino group, through formation of covalent amide bond. By measuring the UV/vis absorption spectra of globular protein (data not shown), there is a strong absorption peak in the wavelength ranging from 200 nm to 230 nm. Obviously, it is generated by the $\pi \rightarrow \pi^*$ transition of carbonyl group (C＝O) in the amide bond, and the strongest absorption of amide bond for ultraviolet light is occurred at about 200 nm. This property will severely hinder the excitation energy of fluorescence to protein within the wavelength range of 200～230 nm. Furthermore, peptide bonds have also been endowed with partial characteristics analogous to double bond, and with the increase of conjugation length in polypeptide chain, bathochromic shift should be appeared ordinarily as a result of absorption induced by $\pi \rightarrow \pi^*$ transition. One logical interpretation for this phenomenon is that the enhancement of electronic mobility in conjugated system could be a trigger for the reduction of energy to molecular orbital, and then the amount of energy required to $\pi \rightarrow \pi^*$ transition will be decreased. In

addition, compared with free amino acids, the microenvironment of Phe, Trp and Tyr residues may change from hydrophilic to hydrophobic when the three amino acid residues are located at the binding domain on protein, such event can inevitably arouse moderately hypsochromic shift of fluorescence emission band in these aromatic amino acid residues. Therefore, these factors enable the fluorescence emission band of Phe, Trp and Tyr residues in protein to form peak 2, and the fluorescence intensity of this peak mostly depends upon the absorbance of amide bonds in protein at ～200 nm. Comparing with the fluorescence intensity of peak 1 and peak 2, in the presence and absence of flavazin, the strength ratio of the two peaks was 1∶1.1 and 1∶1.19, respectively. The decrement of the two peaks in combination with the steady state fluorescence and far-UV CD spectra, affirmed that the molecular recognition of flavazin by albumin awakened the major perturbation of the polypeptide chain of albumin, which resulted in conformational changes of albumin and augmented the baring of some hydrophobic speckles that had been concealed before.

Table 2 here about

Although the above results and elucidations apparently insinuated the binding of flavazin to albumin initiated conformational changes in protein, it is worthwhile to note that the alterations of conformation under the circumstances can not be ascribed to the considerable damage to the three-dimensional structure of albumin. Probably this issue is the self-adjustment of protein conformation so as to accommodate the ligand more suitably. Virtually, the protein is not in a static state, the entire albumin

419 tumbles in approximately 40 ns because of its loop-link structure. And the structural
420 features allow protein fast enlargement, contraction and flexure, some of it inherent
421 and the others associated with binding of substances. Moreover, amino acid side
422 chains of albumin are continual moving on more quick time ranges, for example, the
423 Trp-214 residue side chain rotates individually at a swift rate, about 10^{-10} s rotational
424 correlation time, as portrayed by Munro et al.[47] in a very early study. Consequently,
425 albumin in solution can be deemed to possess a unitary "heart-shaped" overall, but it
426 is possibly more authentic to consider it as an assemblage of peristaltic, springy
427 components, commonly altering in conformation by unwrapping and shutting of their
428 primary fissures. Considering this aspiratory mode, and along with many of its amino
429 acid side chains frequently in motion on a microscale, the protein is perfectly fitted to
430 absorb or release numerous ligands such as flavazin that it transports in the human
431 body.

432 **Recognition Properties.** As previously mentioned, fluorescence quenching has
433 been broadly studied both as a fundamental phenomenon, and as an origin of fact
434 about biological systems. These biochemical utilizations of quenching are owing to
435 the molecular interactions that result in quenching. Therefore, quenching studies can
436 expose the accessibility of fluorophores to quenchers and can also be employed to
437 disclose the localization of fluorophores in proteins and their perviousness to
438 quenchers. To explain the nature of molecular recognition properties of flavazin by
439 albumin, the raw fluorescence data were analyzed according to the well-known
440 Stern-Volmer equation (2), and the corresponding results fitted from the Stern-Volmer

441 plots Fig. 4 were summarized in Table 3. The results suggest that the Stern-Volmer
442 quenching constant K_{SV} is reversely correlated with temperature and the value of k_q is
443 100-fold higher than the maximum value of diffusion-controlled quenching in
444 aqueous media ($\sim 10^{10}$ M^{-1} s^{-1}), indicating that the probable quenching mechanism for
445 albumin Trp residue fluorescence by flavazin is a static type,[48] due to higher
446 temperature will normally result in the dissociation of blandly bound complexes, and
447 accordingly smaller amounts of static quenching.

448 Fig. 4 here about

449 Table 3 here about

450 Static and dynamic quenching could easily be distinguished through their differing
451 dependence on temperature and viscosity, but fluorescence quenching is best studied
452 by fluorescence lifetime measurements, as described by Lakowicz,[23] which can tell
453 apart between static and dynamic processes directly. The representative fluorescence
454 decay patterns of albumin at various molar ratios of flavazin in Tris-HCl buffer, pH＝
455 7.4, are appeared in Fig. S3, and the fluorescence lifetime and their amplitudes are
456 summarized in Table 4. The decay curves fitted well to biexponential function and the
457 relative fluorescence lifetimes being produced are τ_1＝3.41 ns and τ_2＝7.48 ns of
458 albumin, while in the maximum concentration of flavazin, the lifetimes are τ_1＝2.84
459 ns and τ_2＝6.86 ns. As Trp is known to divulge multiexponential decays, we have not
460 tried to assign the independent components, contrariwise, the average lifetime has
461 been employed in order to acquire a qualitative analysis. The average lifetime reduces
462 from 6.06 ns to 5.99 ns, at different concentrations of flavazin, attesting quenching is

really static type, an albumin-flavazin complex is formed between the fluorophore and the ligand, and this complex is non-fluorescent.[49]

Table 4 here about

As we have seen, the physiological function of a protein is decided by its structure, molecular recognition of ligand by normally arouses change to their three-dimensional structures, resulting in an alteration of absorption, hence the form of ligand is regarded as pharmacologically or toxicologically active and its function associates primary with the protein-ligand affinity.[50,51] To evaluate the affinity of flavazin to albumin, equation (3) and (4) was utilized to calculate K and n by linear regression of a plot of the $\log(F_0-F)/F$ *versus* $\log[Q]$ or F_0/F *against* $[Q_t]F_0/(F_0-F)$, and the results were listed in Table 3. Both K values are descended with the arising temperature, bringing about the destabilization of the albumin-flavazin complex. In addition, the value of n derived from equation (3) and (4) is appropriately equal to 1, which may declare the existence of only one kind of binding site in albumin for flavazin. The intrinsic fluorescence of albumin is owing to the lonely Trp-214 in subdomain IIA,[52] from the value of n, ligand binding site is most likely adjacent to this residue, and causing fluorescence quenching. Physiologically, a ligand with a relatively high albumin binding affinity will have a long half-life, which may boost its toxicity; on the contrary, if a ligand with a low albumin affinity is limited in its capacity to perfuse tissues and reach the site of action. This is especially relevant to hydrophobic ligands, in which albumin binding enhances their solubility and subsequent tissue distribution. Consequently, understanding the extent of ligand

affinity will aid in recognizing ligands with poisonous side effect, and we can not disregard this feature, for the degree of ligand binding to both plasma and tissue biomacromolecules is partially rely on both the distinct physicochemical properties of the exceptional chemical and on the character of the plasma and tissue ingredients themselves.[53,54]

As shown in Table 3, only one location in protein to accommodate ligand flavazin, which part of biomacromolecule does it lie in? To answer this we, for one thing, will use competitive binding between the flavazin and other ligands that specifically bind to a known site or domain to tackle the problem. Notably, pioneering work by Sudlow et al.[55,56] found two dominant ligand binding sites on the protein, named site I and site II. Site I is known as the warfarin-azapropazone site, and formed as a cavity in subdomain IIA, the single Trp-214 residue of the protein in this region. The inside wall of the pocket is formed by hydrophobic side chains, whereas the entrance to the hole is surrounded by positively charged residues. The exceptional feature of this site is the binding of the ligand, which is a bulky heterocyclic anion with a negative charge localized in the middle of the molecule, ligands binding in site I include warfarin, phenylbutazone, azapropazone and diflunisal.[57,58] Site II corresponds to the pocket of subdomain IIIA, and is known as the indole-benzodiazepine site, which is almost the same size as site I, the interior of the cavity is constituted by hydrophobic amino acids residues and the exterior pocket presented two imperative amino acids residues (Arg-410 and Tyr-411). Ligands binding to site II are aromatic carboxylic acids with negatively charged acidic group at the end of the molecule, e.g. ibuprofen,

diazepam, flufenamic acid and halothane.[59] Later on Brodersen et al.[60] pointed out that digitoxin binding in albumin is individual from Sudlow's site, and perch on what was nominated as site III. In the current job, the competitors used included warfarin, a characteristic marker for site I, diazepam for site II, digitoxin for site III and hemin for domain I. According to equation (3), the association intensity were plotted from fluorescence data and found to be $(1.054 \pm 0.017) \times 10^4$ M^{-1}, $(4.871 \pm 0.009) \times 10^4$ M^{-1}, $(4.915 \pm 0.021) \times 10^4$ M^{-1} and $(4.792 \pm 0.013) \times 10^4$ M^{-1} for warfarin, diazepam, digitoxin and hemin. The results state obviously that the bound albumin-flavazin complex was mostly affected by warfarin, namely, flavazin shares the identical site with warfarin in albumin, and is also in accordance with hydrophobic ANS probe and protein denaturation with guanidine hydrochloride (GuHCl) placing the flavazin at subdomain IIA, Sudlow's site I.

The fluorescence dye 8-anilino-1-naphthalenesulfonic acid (ANS), which is sensitive to microenvironmental changes and can serve as a suitable messager of conjugation in the neighborhood of protein fluorophore Trp residue, thereby has been frequently employed to characterize all of the hydrophobic binding sites of proteins.[61] To investigate the binding patch thoroughly, binding studies were carried out in the presence of ANS under identical conditions, and the relative fluorescence intensity (F/F_0) *versus* ligand concentration ([Ligand]) plots is denoted in Fig. 5. Distinctly, at a ligand concentration of 7.0 μM, both flavazin and ANS decrease Trp-214 residue fluorescence, but the degree of quenching by flavazin was much less as compared to ANS; ANS could quench about 67.48%, whereas flavazin could only diminish about

529 24.86% of Trp-214 residue fluorescence. Stryer[62] first indicated that the quantum
530 yield of ANS is about 0.002 in aqueous solution, but near 0.4 if the hydrophobic dye
531 bound to protein, with almost no contribution from the unbound probe. When flavazin
532 is added to the albumin-ANS system, it can contend for ANS and displace ANS from
533 its binding site, thus the fluorescence would reduce. It is easy to discern from Fig. 5
534 about 20.14% of ANS fluorescence has vanished, explaining how flavazin can
535 compete against ANS for its binding site. The most basic reason why ANS
536 fluorescence should be decreased is that the dye ANS is essentially non-fluorescent
537 when in aqueous media, but it will become highly fluorescent in nonpolar solvents or
538 when it is bound to proteins. And, although still partly controversial, consensus exists
539 today that there are four hydrophobic binding sites for ANS associated with albumin,
540 but preferentially at a site in subdomain IIIA (Sudlow's site II).[63,64] In the current
541 environment, ANS intensely quenches the fluorescence of albumin, which testifies
542 that the binding location for ANS is in this high-affinity site; also, approximately
543 20.14% displacement of ANS fluorescence attests that flavazin and ANS probe do not
544 share a common site in protein albumin, i.e. Sudlow's site II.

545 Fig. 5 here about

546 Protein unfolding evoked by chemical denaturants such as urea or guanidine
547 hydrochloride (GuHCl) is a common accepted method to probe the conformational
548 stability of proteins by estimating the imparities in spatial structure between the
549 folded and the denatured states. Meantime, it has been displayed that low
550 concentrations of denaturants might give rise to protein denaturation as there are an

enormous number of equivalent and noninteracting binding sites on the denatured structure than there are on the native conformation.[65] To examine the binding domain of flavazin in greater detail, chemical unfolding of protein experiments was executed by using GuHCl as a typical denaturant. Based on the previous story of Ahmad et al.,[66] GuHCl caused albumin unfolding comes to pass in multiple steps. At 1.4 M GuHCl, only domain III is completely unfolded, the existence of a molten globule-like intermediate state of domain III around 1.8 M GuHCl concentration and at 3.2 M GuHCl, domain I is departed from the domain II, and domain I is wholly unfolded while domain II is partly. This result has been proved by Galantini et al.,[67] who applied a small-angle X-ray scattering and light scattering techniques to expound the unfolding picture of fatted and defatted albumin. In the current study, samples of varied GuHCl were prepared by blending different molar ratios of GuHCl stock solution and Tris-HCl buffer of pH＝7.4. The final solution mixture was incubated with various GuHCl concentrations for 12 h at room temperature before steady state fluorescence measurements. Equation (3) was used utilized to generate the association strength in the presence of different concentrations of GuHCl, and the values were found to be $(4.581\pm0.008)\times10^4$ M^{-1}, $(3.316\pm0.014)\times10^4$ M^{-1} and $(0.2094\pm0.011)\times10^4$ M^{-1} for flavazin at 1.4 M, 1.8 M and 3.2 M GuHCl, respectively. This result illustrates obviously that the unfolding of domain II conspicuously affects the flavazin binding to albumin, but unfolding of domain III will have little or no effect on the recognition ability of albumin for ligand flavazin.

Molecular Docking. Molecular docking is presuming a mounting significant

function in realizing the foundation of ligand-biopolymer recognitions and the object of ligand-protein docking is to logical deduce the paramount binding mode of a ligand with a protein of known three-dimensional structure. To explain recognition mode between flavazin and albumin more fully, molecular docking was conducted and the best docking energy results are expressed in Fig. 6. According to X-ray crystallographic analyses of albumin,[58,59] it is a single, non-glycosylated polypeptide chain of 585 amino acid residues that organizes to form a heart-shaped protein with dimensions 80 Å×80 Å×80 Å and with a thickness of 30 Å. Albumin is composed of three homologous domains (I, II and III): I (residues 1-195), II (196-383) and III (384-585), each of which has two subdomains (A and B) with distinct helical folding patterns that are connected by flexible loops. High-affinity ligand binding generally takes place to Sudlow's site I and site II, using Sudlow's nomenclature, which corresponds to subdomain IIA and IIIA of the protein.

It will clearly be seen that ligand flavazin was located at subdomain IIA formed by six-helices (Fig. 6(A)), the molecular distance between the center of benzene ring (A-ring) in flavazin and the heart of indole ring in Trp-214 is 2.52 Å, which manifested evidently the existence of parallel π-π interactions between ligand and albumin (Fig. 6(B)). Also, on the basis of surface modification of amino acid residues comprised of subdomain IIA, we can telling disclose a hydrophobic patch within the domain constituted by Lys-195, Leu-198, Trp-214, Arg-222, Val-343, Lys-436, Tyr-452 and Leu-481, the hydrophobic group in flavazin such as benzene ring toward the region, this phenomenon suggests the presence of evident hydrophobic

595 interactions between them (Fig. 6(C)). Moreover, the nitrogen atoms N-1 and N-2 of
596 azo group, the oxygen atom (O-3) of hydrogen group and the oxygen atom (O-4) of
597 sulphonyl group in flavazin can make strong hydrogen bonds with the hydrogen atom
598 of secondary amine group in Trp-214, the hydrogen atom of amino group in Arg-222
599 and the hydrogen atom of amino group in Lys-436 residues, and the bond length,
600 respectively, is 3.03 Å, 2.57 Å, 3.05 Å and 2.43 Å. The hydrogen bond assists as an
601 "anchor", which extremely determines the three-dimensional space position of
602 flavazin in the subdomain IIA, and stimulates the hydrophobic interactions of the
603 benzene ring and peptide bond with the side chain of albumin.

604 Based on the molecular docking described above, we came to the rational
605 conclusion that ligand flavazin was situated within Sudlow's site I, and the main
606 driving forces in the albumin-flavazin molecular recognition are π-π, hydrophobic
607 interactions and hydrogen bonds. The spatial structure of biopolymer was also
608 disturbed by flavazin with a partial destabilization of protein. Likewise, the computed
609 Gibbs free energy from computational docking is $\Delta G° = -26.76$ kJ mol^{-1} and is
610 highly approaching the experimental value $\Delta G° = -26.85$ kJ mol^{-1}, signifying the
611 recognition process was an exothermic reaction and the believability of the
612 experimental results of steady state fluorescence examination.

613 Fig. 6 here about

614 **Molecular Dynamics Simulation.** Molecular dynamics (MD) simulation is the
615 most comprehensive computational method that allows one to predict the time
616 assessment of a molecular system of interacting particles, and it has also supplied

detailed knowledge on the fluctuations and conformational alterations of macromolecules such as protein.[68] In order to further validate the rationality of the molecular docking and the structural stability of the albumin-flavazin complex, MD simulation has been carried out using Gromacs 4.5.5 versatile package. Typically, for simulations of proteins, a stable simulation is demanded, often mirroring some kind of equilibrium of the protein-ligand recognition system. Therefore, several criteria of stability are requested and, the most accepted of these standards is the Root-Mean-Square Deviation (RMSD) of C_α atoms from the initial (usually X-ray diffraction) starting structure.[69] In the current study of globular protein albumin conformations, we normally detects the comparability in three-dimensional structure by the RMSD data of the backbone C_α atomic coordinates after optimal rigid body superposition. If the RMSD did not fluctuate noticeably to some extent in a reasonable time, the system can be regarded as the achievement of equilibrium states. Fig. 7 exhibits the RMSD of the backbone C_α atoms of albumin (Fig. 7(A)), and the flavazin and the backbone C_α atoms of albumin (Fig. 7(B)) from MD simulations at 298 K. Obviously, the RMSD of unmixed albumin (Fig. 7(A)) floats steadily since 2,000 ps, and the amplitude is within a range of 0.05 nm. While for albumin-flavazin adduct (Fig. 7(B)), it is distinct that the system reaches stable and balanced starting from the time point 2,400 ps till the end of the MD simulation, 10,000 ps.

Fig. 7 here about

The average stable conformations between 6,000 ps and 10,000 ps after equilibration were selected and overlapped original conformations (Fig. 8(A)).

Evidently, the initial conformation overlap the average conformation at equilibrium very well, and there are no conformation flipped and bent could be observed. Furthermore, several crucial noncovalent interactions, such as π-π, hydrophobic interactions and hydrogen bonds still remains paramount, but the strength of the noncovalent bonds has subtle differences between the two conformations (Fig. 8(B)). For example, notable π-π interactions exists in the A-ring of flavazin and the indole ring in Trp-214 residue, the perpendicular distance is 2.55 Å. Due to the better superposition of the average and original conformations, the hydrophobic amino acid residues, e.g. Lys-195, Leu-198, Trp-214, Arg-222, Val-343, Lys-436, Tyr-452 and Leu-481 also surrounds the ligand flavazin thorough MD simulation, thereby denoting the existence of obvious hydrophobic interactions between flavazin and protein. In addition, the two hydrogen bonds between the nitrogen atoms N-1 and N-2 of azo group and the hydrogen atom of secondary amine group in Trp-214 residue have shown some enhancement, intuitively, the bond lengths decrease from 3.03 Å and 2.57 Å to 3.01 Å and 2.52 Å, respectively; while the hydrogen bonds between the oxygen atom O-3 and O-4 of hydroxyl group and sulphonyl group, respectively, and the hydrogen atoms of amino group in Arg-222 and Lys-436 residues have grown thin, the bond lengths, respectively, change from 3.05 Å and 2.43 Å to 3.11 Å and 2.70 Å.

Fig. 8 here about

Besides, the Root-Mean-Square Fluctuation (RMSF) is beneficial for illustrating local changes along the protein polypeptide chain. It is classically computed for the C_α atom of each residue and is thereafter plainly the square root of the variance of the

fluctuation around the average position. Accordingly, a plot of RMSF *against* residue number (Fig. 9) indicates the regions of high flexibility as peaks in the plot. As shown in Fig. 9, we contrasted the RMSF of amino acid residues between single albumin and the albumin-flavazin complex, it will be found that the RMSF of amino acid residues (residues 199－292, subdomain IIA) in albumin-flavazin adduct is significantly greater than the corresponding amino acid residues in pure albumin. The most striking feature of this issue is the RMSF of amino acid residues in pure albumin is much less than the identical amino acid residues, which are continual with Trp-214 and Arg-222 residues in the albumin-flavazin conjugates. Actually, these phenomena arise from the fact that the noncovalent interactions between Trp-214 and Arg-222 residues and flavazin are relatively strong, then the dynamic change of flavazin can probably arouse larger displacement for relevant amino acid residues in albumin during the whole MD simulations. Nevertheless, some amino acid residues, which lie outside the subdomain IIA, such as Lys-436 (subdomain IIIA, helix 3) and those connected with Lys-436 residue have also fair apparent alterations in conformation. This suggests that the changes of amino acid residues around flavazin are more remarkable after the protein-ligand complex formation. In other words, flavazin, in a manner, would influence the regularly structure of protein polypeptide chain, and these impacts represented the variations of protein spatial conformational modifications. Taking all the above MD simulations into consideration, we could clearly see that the results of molecular docking are logically reliable, and further testify that flavazin located at the subdomain IIA in albumin stably, and forms a protein-flavazin noncovalent complex

683 primarily through π-π, hydrophobic interactions and hydrogen bonds.[70,71] These
684 noncovalent bonds have caused the conformational changes in protein, which is
685 compatible with foregoing results came from steady state fluorescence, CD spectra as
686 well as detailed analyses of three-dimensional fluorescence.

687 Fig. 9 here about

688

689 **CONCLUDING REMARKS**

690

691 With respect to human health, the most straight and most dangerous influence is
692 the contact to pathogens or to chemical poisons through the consumer commodities or
693 food chain, e.g. the consequence of irrigating crops with contaminated water and of
694 bioaccumulation of noxious compounds such as pesticides or colorants by aquatic life,
695 involving seafood and fish.[72-75] As has been argued, azo colorants are complicated
696 organic compounds that were primitively sprung from color tar, but nowadays from
697 petroleum. Many companies around the world adore utilizing them because they are
698 cheaper, more stable and brilliant than most natural colorants. This task delineates
699 herein an integrated experimental and computational docking survey of the
700 recognition of a model azo compound flavazin by a very pivotal albumin in aqueous
701 buffer at physiological pH＝7.4. The data of steady state fluorescence, far-UV CD
702 and three-dimensional fluorescence unmistakably testified the albumin spatial
703 structure changes after the increment of flavazin with a shrink in α-helix following by
704 an amplify in β-sheet, turn and random coil, initiating albumin conformational

interruption. We surmised that the disturbance of albumin might probably be originated from oxidative stress by the formation of free radicals. There is a frank *in vivo* proof that after treating laboratory rats with flavazin analogue – tartrazine, which is a synthetic lemon yellow azo compound greatly employed as a food coloring, this agent can be reduced into aromatic amine by intestinal bacteria (flora) and the formed aromatic amines may further engender reactive oxygen species (ROS) in liver, blood stream and kidney as portion of their metabolism by reaction of these amino groups with nitrite or nitrite containing foods or in the stomach.[13] The ROS such as superoxide anion, hydroxyl radical and hydrogen peroxide could also be yielded in the degradation of nitrosamines and augment oxidative stress. This phenomenon wonderfully harmonizes an earlier upshot where sodium dodecyl sulfate-polyacrylamide gel electrophoresis was used for the inspection of albumin-fungicide thiophanate-methyl recognition.[76] Yet, the vigorous signal at 208 nm exhibits the existence of a voluminous amount of α-helix in protein, which is still capable of fastening flavazin, and the destabilization of albumin thus does not purport a partial damage but adaptation on the spatial structure.

Still, steady state and time-resolved fluorescence determinations have proclaimed ligand flavazin recognizes by albumin was the formation of albumin-flavazin complex via π-π, hydrophobic interactions and hydrogen bonds with an association strength of 10^4 M^{-1}. According to hydrophobic ANS probe, GuHCl induced denaturation of protein and molecular docking, subdomain IIA was allocated the binding cavity for the flavazin on albumin, this was further proved by site-specific ligands outcomes,

727 which dug out warfarin, a characteristic marker ligand of Sudlow's site I, competed
728 with flavazin for the site. Via MD simulations, we may confirm that the molecular
729 docking results are believable, and the amino acid residues, i.e. Trp-214, Arg-222 and
730 Lys-436 were found to be pivotal in the molecular recognition of flavazin by protein.
731 It is noticeable that the recognition ability of protein albumin with flavazin belongs to
732 moderate affinity, as compared with other powerful protein-ligand system with
733 intensity ranging from 10^6 to 10^8 M^{-1},[77] but the physiological concentration of
734 albumin is actually ample enough (~640 μM) to allow flavazin vastly binding.
735 Albumin binding could essentially elongate the *in vivo* half-life of azo compounds,
736 and the concentration of azo chemicals universally bioaccumulated in liver, kidney
737 and plasma and eventually, the reduction and metabolism of azo colorants by various
738 enzymes such as human cytochrome P450 enzyme in the human body may surely
739 generate more toxicity than the parent compound for human health.[78,79] For example,
740 intensive occupational touch to 4-aminobiphenyl and benzidine can bring about
741 urinary bladder cancer in workers; the identical reduction chemical 4-aminobiphenyl
742 is also exist in cigarette smoke, it was seriously noticed smokers were at huge risk not
743 only of heart disease and lung cancer, but also of urinary bladder cancer, recounted in
744 a little earlier description by Weston et al.[80] and Skipper et al.[81,82]

745 Altogether, all the consequences and discussions emerged in this contribution
746 meet well with the situation that allied application of multiple spectroscopic and
747 molecular docking and MD simulations are beneficial to decipher the ligands such as
748 azo compounds molecular recognition by biomacromolecule. Even though our works

749 do not correlate directly *in vivo* bioassay, it lends momentous insight to the molecular
750 recognition of the toxic azo colorants by typical mammalian protein, due to albumin is
751 possibly the most vital functional macromolecule for various ligands in human plasma,
752 under physiological conditions, to recognize almost any pharmaceutical or
753 toxicological agents and its metabolites to the target tissue, where it elicits its
754 biological activity. On the other hand, we should pay more particularly attention to
755 this issue regarding ligand-biomacromolecule molecular recognition, since ligands
756 usually combine either reversibly or irreversibly with action positions on intrastitial
757 biopolymers or organelles, and by this means induce variations of physicochemical or
758 biochemical procedures in the human beings.

AUTHOR INFORMATION

Corresponding Author

*E-mail: alexf.ting@gmail.com, feiding@cau.edu.cn (F. Ding); pyk2009@nwsuaf.edu.cn (Y.-K. Peng). Phone/fax: +86-29-87092367.

FUNDING

This work was executed under the auspices of the National Natural Science Foundation of China (No. 31171693).

NOTES

The authors declare no competing financial interest.

ACKNOWLEDGEMENTS

We are particularly indebted to Professor Ulrich Kragh-Hansen of Department of Medical Biochemistry, University of Aarhus, for the priceless gift of his doctoral dissertation. We are very grateful to Miss Wei Liu for her salutary contribution in language refinement and manuscript melioration. We thank Professor Cesar G. Fraga of School of Pharmacy and Biochemistry, University of Buenos Aires, for his kindly support during the manuscript processing. Thanks also go to the reviewers of this manuscript for their insightful comments.

ABBREVIATIONS USED

ANS, 8-anilino-1-naphthalenesulfonic acid; Arg, arginine; CD, circular dichroism; GuHCl, guanidine hydrochloride; IRF, instrument response function; Leu, leucine; Lys, lysine; MD simulation, molecular dynamics simulation; NPT, isothermal-isobaric; Phe, phenylalanine; PME, Particle Mesh Ewald; R, correlation coefficient; RMSD, Root-Mean-Square Deviation; RMSF, Root-Mean-Square Fluctuation; ROS, reactive oxygen species; S.D., standard deviation; Tris, tris(hydroxymethyl)aminomethane; Trp, tryptophan; Tyr, tyrosine; UV/vis, ultraviolet-visible spectroscopy; Val, valine.

REFERENCES

1. R. E. Wrolstad and C. A. Culver, *Annu. Rev. Food Sci. Technol.*, 2012, **3**, 59-77.
2. M. Stock and S. Dunn, *J. Phys. Chem. C*, 2012, **116**, 20854-20859.
3. N. A. Travlou, G. Z. Kyzas, N. K. Lazaridis and E. A. Deliyanni, *Langmuir*, 2013, **29**, 1657-1668.
4. L.-H. Ahlström, C. S. Eskilsson and E. Björklund, *Trends Anal. Chem.*, 2005, **24**, 49-56.
5. T. M. Parkinson and J. P. Brown, *Annu. Rev. Nutr.*, 1981, **1**, 175-205.
6. J. Araña, D. Zerbani, J. A. H. Melián, D. G. Sousa, O. G. Díaz and J. M. D. Rodríguez, *Photochem. Photobiol. Sci.*, 2013, **12**, 703-708.
7. M. A. Brown and S. C. DeVito, *Crit. Rev. Environ. Sci. Technol.*, 1993, **23**, 249-324.
8. K. Golka, S. Kopps and Z. W. Myslak, *Toxicol. Lett.*, 2004, **151**, 203-210.
9. D. McCann, A. Barrett, A. Cooper, D. Crumpler, L. Dalen, K. Grimshaw, E. Kitchin, K. Lok, L. Porteous, E. Prince, E. Sonuga-Barke, J. O. Warner and J. Stevenson, *Lancet*, 2007, **370**, 1560-1567.
10. S. Kobylewski and M. F. Jacobson, *Int. J. Occup. Environ. Health*, 2012, **18**, 220-246.
11. M. Poul, G. Jarry, M. O. Elhkim and J.-M. Poul, *Food Chem. Toxicol.*, 2009, **47**, 443-448.

12. http://www.efsa.europa.eu/en/press/news/ans100726.htm
13. K. A. Amin, H. A. Hameid II and A. H. A. Elsttar, *Food Chem. Toxicol.*, 2010, **48**, 2994-2999.
14. A. Yadav, A. Kumar, P. D. Dwivedi, A. Tripathi and M. Das, *Toxicol. Lett.*, 2012, **208**, 239-245.
15. C.-a. Hsu, T.-N. Wen, Y.-C. Su, Z.-B. Jiang, C.-W. Chen and L.-F. Shyur, *Environ. Sci. Technol.*, 2012, **46**, 5109-5117.
16. L. Abramsson-Zetterberg and N.-G. Ilbäck, *Food Chem. Toxicol.*, 2013, **59**, 86-89.
17. J. W. Li, P. Nowak and S. Otto, *J. Am. Chem. Soc.*, 2013, **135**, 9222-9239.
18. R. Baron and J. A. McCammon, *Annu. Rev. Phys. Chem.*, 2013, **64**, 151-175.
19. U. Kragh-Hansen, *Pharmacol. Rev.*, 1981, **33**, 17-53.
20. J. Z. Chen and D. S. Hage, *Nat. Biotechnol.*, 2004, **22**, 1445-1448.
21. J. Anguizola, K. S. Joseph, O. S. Barnaby, R. Matsuda, G. Alvarado, W. Clarke, R. L. Cerny and D. S. Hage, *Anal. Chem.*, 2013, **85**, 4453-4460.
22. L. Turell, H. Botti, S. Carballal, G. Ferrer-Sueta, J. M. Souza, R. Durán, B. A. Freeman, R. Radi and B. Alvarez, *Biochemistry*, 2008, **47**, 358-367.
23. J. R. Lakowicz, *Principles of Fluorescence Spectroscopy*, third ed.; Springer Science＋Business Media: New York, 2006, pp. 63-606.
24. S. Sugio, A. Kashima, S. Mochizuki, M. Noda and K. Kobayashi, *Protein Eng.*, 1999, **12**, 439-446.
25. P. A. Holt, J. B. Chaires and J. O. Trent, *J. Chem. Inf. Model.*, 2008, **48**, 1602-1615.

26. M. J. D. Powell, *Comput. J.*, 1964, **7**, 155-162.

27. R. Spitzer and A. N. Jain, *J. Comput.-Aided Mol. Des.*, 2012, **26**, 687-699.

28. M. A. Lill and M. L. Danielson, *J. Comput.-Aided Mol. Des.*, 2011, **25**, 13-19.

29. B. Hess, C. Kutzner, D. van der Spoel and E. Lindahl, *J. Chem. Theory Comput.*, 2008, **4**, 435-447.

30. S. Pronk, S. Páll, R. Schulz, P. Larsson, P. Bjelkmar, R. Apostolov, M. R. Shirts, J. C. Smith, P. M. Kasson, D. van der Spoel, B. Hess and E. Lindahl, *Bioinformatics*, 2013, **29**, 845-854.

31. D. M. F. van Aalten, R. Bywater, J. B. C. Findlay, M. Hendlich, R. W. W. Hooft and G. Vriend, *J. Comput.-Aided Mol. Des.*, 1996, **10**, 255-262.

32. W. L. Jorgensen, J. Chandrasekhar, J. D. Madura, R. W. Impey and M. L. Klein, *J. Chem. Phys.*, 1983, **79**, 926-935.

33. K. Ikeda, *Prog. Theor. Phys.*, 1967, **38**, 584-610.

34. T. Darden, D. York and L. Pedersen, *J. Chem. Phys.*, 1993, **98**, 10089-10092.

35. B. Hess, H. Bekker, H. J. C. Berendsen and J. G. E. M. Fraaije, *J. Comput. Chem.*, 1997, **18**, 1463-1472.

36. W. Humphrey, A. Dalke and K. Schulten, *J. Mol. Graph.*, 1996, **14**, 33-38.

37. P. Bourassa, S. Dubeau, G. M. Maharvi, A. H. Fauq, T. J. Thomas and H. A. Tajmir-Riahi, *Biochimie*, 2011, **93**, 1089-1101.

38. O. K. Abou-Zied, N. Al-Lawatia, M. Elstner and T. B. Steinbrecher, *J. Phys. Chem. B*, 2013, **117**, 1062-1074.

39. G. Scatchard, *Ann. N. Y. Acad. Sci.*, 1949, **51**, 660-672.

40. P. Singh and P. K. Chowdhury, *J. Phys. Chem. Lett.*, 2013, **4**, 2610-2617.

41. O. K. Abou-Zied, *RSC Adv.*, 2013, **3**, 8747-8755.

42. D. Charbonneau, M. Beauregard and H.-A. Tajmir-Riahi, *J. Phys. Chem. B*, 2009, **113**, 1777-1784.

43. J. Rohacova, G. Sastre, M. L. Marin and M. A. Miranda, *J. Phys. Chem. B*, 2011, **115**, 10518-10524.

44. L. Whitmore and B. A. Wallace, *Biopolymers*, 2008, **89**, 392-400.

45. D. Agudelo, P. Bourassa, J. Bruneau, G. Bérubé, É. Asselin and H.-A. Tajmir-Riahi, *PLOS ONE*, 2012, **7**, e43814.

46. M. R. Eftink and C. A. Ghiron, *Anal. Biochem.*, 1981, **114**, 199-227.

47. I. Munro, I. Pecht and L. Stryer, *Proc. Natl. Acad. Sci. U. S. A.*, 1979, **76**, 56-60.

48. A. Tarushi, J. Kljun, I. Turel, A. A. Pantazaki, G. Psomas and D. P. Kessissoglou, *New J. Chem.*, 2013, **37**, 342-355.

49. O. K. Abou-Zied and N. Al-Lawatia, *ChemPhysChem*, 2011, **12**, 270-274.

50. M. K. Gilson and H.-X. Zhou, *Annu. Rev. Biophys. Biomol. Struct.*, 2007, **36**, 21-42.

51. L. A. MacManus-Spencer, M. L. Tse, P. C. Hebert, H. N. Bischel and R. G. Luthy, *Anal. Chem.*, 2010, **82**, 974-981.

52. X. M. He and D. C. Carter, *Nature*, 1992, **358**, 209-215.

53. O. Bodansky, *Annu. Rev. Biochem.*, 1948, **17**, 303-326.

54. J. P. F. Bai and D. R. Abernethy, *Annu. Rev. Pharmacol. Toxicol.*, 2013, **53**, 451-473.

55. G. Sudlow, D. J. Birkett and D. N. Wade, *Mol. Pharmacol.*, 1975, **11**, 824-832.

56. G. Sudlow, D. J. Birkett and D. N. Wade, *Mol. Pharmacol.*, 1976, **12**, 1052-1061.

57. T. Peters Jr., *Adv. Protein Chem.*, 1985, **37**, 161-245.

58. J. Ghuman, P. A. Zunszain, I. Petitpas, A. A. Bhattacharya, M. Otagiri and S. Curry, *J. Mol. Biol.*, 2005, **353**, 38-52.

59. D. C. Carter and J. X. Ho, *Adv. Protein Chem.*, 1994, **45**, 153-203.

60. R. Brodersen, T. Sjödin and I. Sjöholm, *J. Biol. Chem.*, 1977, **252**, 5067-5072.

61. C.-G. Rosen and G. Weber, *Biochemistry*, 1969, **8**, 3915-3920.

62. L. Stryer, *J. Mol. Biol.*, 1965, **13**, 482-495.

63. L. A. Bagatolli, S. C. Kivatinitz, F. Aguilar, M. A. Soto, P. Sotomayor and G. D. Fidelio, *J. Fluoresc.*, 1996, **6**, 33-40.

64. D. I. Cattoni, S. B. Kaufman and F. L. G. Flecha, *Biochim. Biophys. Acta – Proteins Proteomics*, 2009, **1794**, 1700-1708.

65. O. B. Ptitsyn, *Adv. Protein Chem.*, 1995, **47**, 83-229.

66. B. Ahmad, M. Z. Ahmed, S. K. Haq and R. H. Khan, *Biochim. Biophys. Acta – Proteins Proteomics*, 2005, **1750**, 93-102.

67. L. Galantini, C. Leggio and N. V. Pavel, *J. Phys. Chem. B*, 2008, **112**, 15460-15469.

68. M. Karplus and J. A. McCammon, *Nat. Struct. Biol.*, 2002, **9**, 646-652.

69. S. B. Dixit, S. Y. Ponomarev and D. L. Beveridge, *J. Chem. Inf. Model.*, 2006, **46**, 1084-1093.

70. O. K. Abou-Zied, *Phys. Chem. Chem. Phys.*, 2012, **14**, 2832-2839.

71. O. K. Abou-Zied, J. Husband, N. Al-Lawatia and T. B. Steinbrecher, *Phys. Chem. Chem. Phys.*, 2014, **16**, 61-70.

72. K. Kümmerer, *Annu. Rev. Environ. Resour.*, 2010, **35**, 57-75.

73. J. N. Seiber and L. A. Kleinschmidt, *J. Agric. Food Chem.*, 2011, **59**, 7536-7543.

74. J. D. Barak and B. K. Schroeder, *Annu. Rev. Phytopathol.*, 2012, **50**, 241-266.

75. K. Armbrust, M. Burns, A. N. Crossan, D. A. Fischhoff, L. E. Hammond, J. J. Johnston, I. Kennedy, M. T. Rose, J. N. Seiber and K. Solomon, *J. Agric. Food Chem.*, 2013, **61**, 4676-4691.

76. Q. Saquib, A. A. Al-Khedhairy, S. A. Alarifi, S. Dwivedi, J. Mustafa and J. Musarrat, *Int. J. Biol. Macromol.*, 2010, **47**, 60-67.

77. M. L. Hall, W. L. Jorgensen and L. Whitehead, *J. Chem. Inf. Model.*, 2013, **53**, 907-922.

78. F. P. Guengerich and Q. Cheng, *Pharmacol. Rev.*, 2011, **63**, 684-699.

79. T. B. Zanoni, T. M. Lizier, M. das D. Assis, M. V. B. Zanoni and D. P. de Oliveira, *Food Chem. Toxicol.*, 2013, **57**, 217-226.

80. A. Weston, N. E. Caporaso, K. Taghizadeh, R. N. Hoover, S. R. Tannenbaum, P. L. Skipper, J. H. Resau, B. F. Trump and C. C. Harris, *Cancer Res.*, 1991, **51**, 5219-5223.

81. P. L. Skipper and S. R. Tannenbaum, *Environ. Health Perspect.*, 1994, **102**, 17-21.

82. P. L. Skipper, S. R. Tannenbaum, R. K. Ross and M. C. Yu, *Cancer Epidemiol. Biomarkers Prev.*, 2003, **12**, 503-507.

Figure captions:

Fig. 1. The ribbon model of the albumin derived from X-ray crystallography (PDB: 1AO6) and the subdivision of albumin into domain (I, II and III) and subdomains (A and B) is indicated. C and N show the C-terminal and N-terminal ends, respectively. This illustration was made with PyMOL on the basis of the atomic coordinates available at the Brookhaven Protein Data Bank (http://www.rcsb.org/pdb).

Fig. 2. Molecular structure of flavazin.

Fig. 3. Fluorescence emission spectra of albumin (1.0 μM) at λ_{ex}＝295 nm (pH＝7.4, T＝298 K) in the presence of different concentrations of flavazin; concentration (μM): 0 (black), 1.0 (red), 2.0 (green), 3.0 (blue), 4.0 (cyan), 5.0 (magenta), 6.0 (yellow) and 7.0 (dark yellow); (x) 7.0 μM flavazin only.

Fig. 4. Stern-Volmer plot describing albumin Trp quenching at pH＝7.4 caused by flavazin association. Fluorescence emission intensity was recorded at λ_{ex}＝295 nm and the λ_{em} maximum occurred at 350 nm. All data were corrected for quencher fluorescence and each data was the mean of three individual experiments±S.D. ranging 0.41%－6.62%.

Fig. 5. Fluorescence quenching patterns of albumin and ANS-albumin system at pH＝

7.4, T＝298 K. Binding isotherm of flavazin (■) and ANS (●) caused quenching of albumin Trp fluorescence (panel (A)) and quenching of ANS-albumin adduct fluorescence (panel (B)) by flavazin (■). All data were corrected for quencher fluorescence. Each data was the mean of three individual measurements ± S.D. ranging 0.16%－5.67%.

Fig. 6. Molecular docking of flavazin docked to albumin. Panel (A) shows docked flavazin into albumin at active site (subdomain IIA), albumin represented in surface colored in red, to flavazin, colored as per the atoms and possess translucent surface of electron spin density. Panel (B) displays the amino acid residues involved in binding of flavazin; the ball-and-stick model indicates flavazin, colored as per the atoms and the key amino acid residues around flavazin has been depicted in stick model, pink stick model reveals hydrogen bonds between Trp-214, Arg-222 and Lys-436 residues and flavazin; green stick model explains hydrophobic interactions between Lys-195, Leu-198, Trp-214, Arg-222, Val-343, Lys-436, Tyr-452 and Leu-481 residues and flavazin. Panel (C) denotes hydrophobic interactions between the amino acid residues composed of subdomain IIA and flavazin molecule. (For interpretation of the references to color in this figure legend, the reader is referred to the web version of the article.)

Fig. 7. Calculated Root-Mean-Square Deviation (RMSD) from the initial X-ray crystal structure for the backbone C_α atoms of albumin (panel (A)) and the flavazin

and the backbone C_α atoms of albumin (panel (B)) from MD simulations at temperature of 298 K with respect to their docking results as a function of the simulation time. The red and blue trajectories represent RMSD values for flavazin and the backbone C_α atoms of albumin, respectively.

Fig. 8. Superposition of the average conformations of MD simulations on the original conformation of molecular docking resulting from albumin-flavazin adduct. Panel (A) shows the initial and average conformation of albumin-flavazin, protein displayed in surface colored in cyan (initial) and mauve (average), respectively, and the original and average conformation of flavazin denoted in grey and green ball-and-stick model. Panel (B) expresses the important amino acid residues involved in the albumin-flavazin recognition process, and the three amino acid residues, which are involved in the formation of hydrogen bonds act as average conformation. (For interpretation of the references to color in this figure legend, the reader is referred to the web version of the article.)

Fig. 9. Root-Mean-Square Fluctuation (RMSF) of the backbone of each residue atomic positions for the unbound (red) and bound (olive) albumin as a function of the atom location along the polypeptide chain.

Table 1
Secondary structure components of albumin recognition with flavazin at pH＝7.4 assessed by Jasco Spectra Manager II Software

Samples	Secondary structure components (%)			
	α-helix	β-sheet	Turn	Random
Free albumin	59.2	7.9	13.5	19.4
Albumin＋flavazin (1∶1)	54.3	8.5	14.6	22.6
Albumin＋flavazin (1∶2)	48.6	9.4	16.1	25.9

Table 2
Three-dimensional fluorescence spectral characteristic parameters of albumin and albumin-flavazin complex

Peaks	Albumin			Albumin-flavazin		
	Peak position $\lambda_{ex}/\lambda_{em}$ (nm/nm)	Stokes $\Delta\lambda$ (nm)	Intensity F	Peak position $\lambda_{ex}/\lambda_{em}$ (nm/nm)	Stokes $\Delta\lambda$ (nm)	Intensity F
Fluorescence peak 1	280.0/347.0	67.0	973.0	280.0/349.0	69.0	881.6
Fluorescence peak 2	230.0/345.0	115.0	459.8	230.0/349.0	119.0	387.7

Table 3
Stern-Volmer (K_{SV}), bimolecular quenching constants (k_q) and affinity (K) for the molecular recognition of albumin with flavazin

T (K)	K_{SV} ($\times 10^4$ M^{-1})	k_q ($\times 10^{12}$ M^{-1} s^{-1})	R^a	K ($\times 10^4$ M^{-1}) (R^a)		n	
				Equation (3)	Equation (4)	Equation (3)	Equation (4)
298	5.039	8.315	0.9994	5.082 (0.9997)	3.944 (0.9986)	1.00	0.98
302	4.787	7.899	0.9996	3.192 (0.9998)	2.591 (0.9991)	0.97	0.97
306	4.481	7.394	0.9997	2.143 (0.9996)	1.337 (0.9989)	0.95	0.94
310	4.205	6.939	0.9995	1.321 (0.9997)	0.8185 (0.9994)	0.92	0.90

[a] R is the correlation coefficient.

Table 4
Fluorescence lifetime of albumin as a function of concentrations of flavazin

Samples	τ_1 (ns)	τ_2 (ns)	A_1	A_2	τ (ns)	χ^2
Free albumin	3.41	7.48	0.35	0.65	6.06	1.03
Albumin＋flavazin (1∶1)	3.31	7.34	0.33	0.67	6.01	1.09
Albumin＋flavazin (1∶2)	3.15	7.21	0.3	0.7	5.99	0.99
Albumin＋flavazin (1∶4)	3.02	7.03	0.25	0.75	6.03	1.01
Albumin＋flavazin (1∶8)	2.84	6.86	0.21	0.79	6.02	1.05

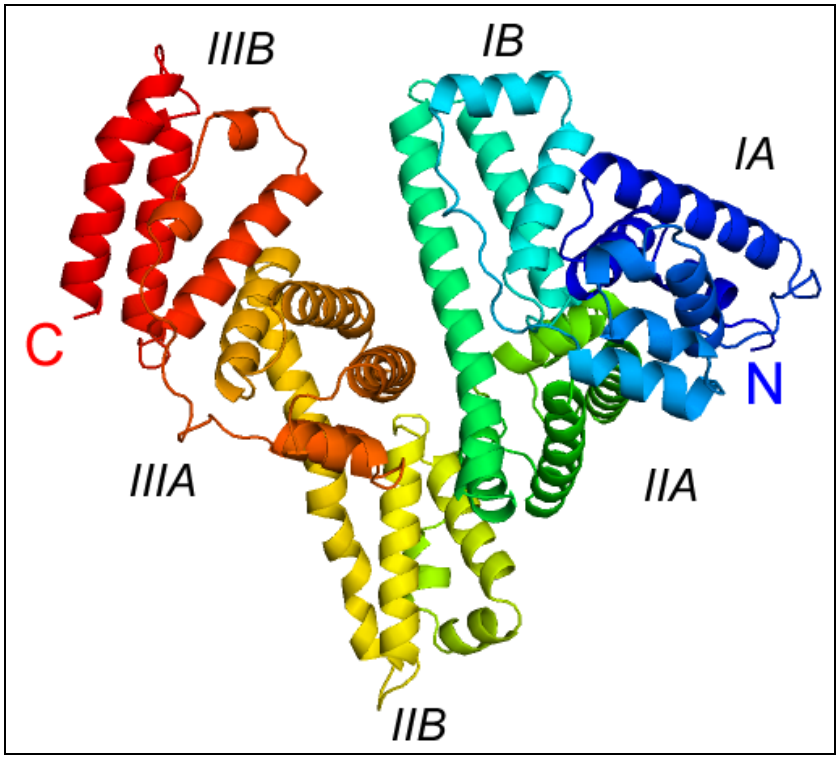

Fig. 1

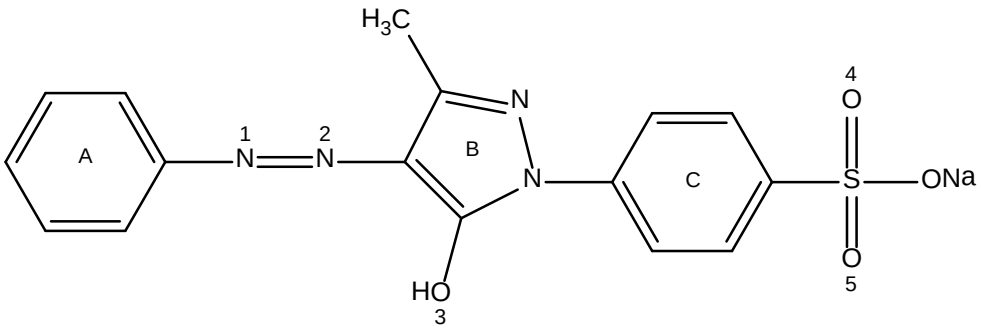

Fig. 2

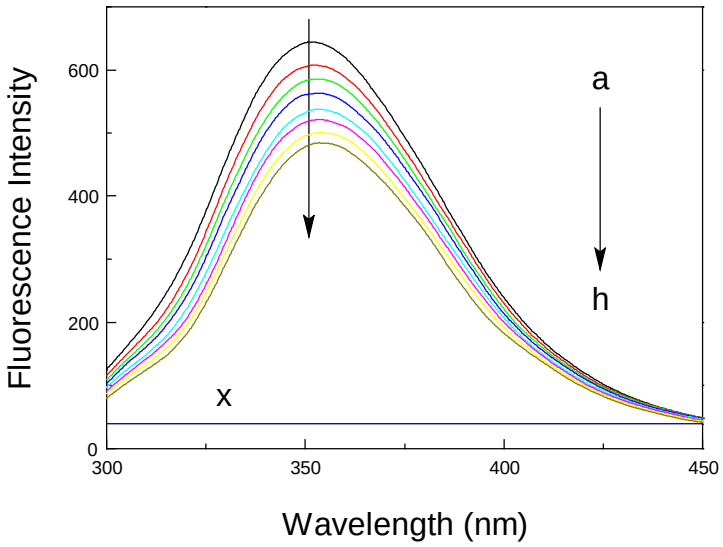

Fig. 3

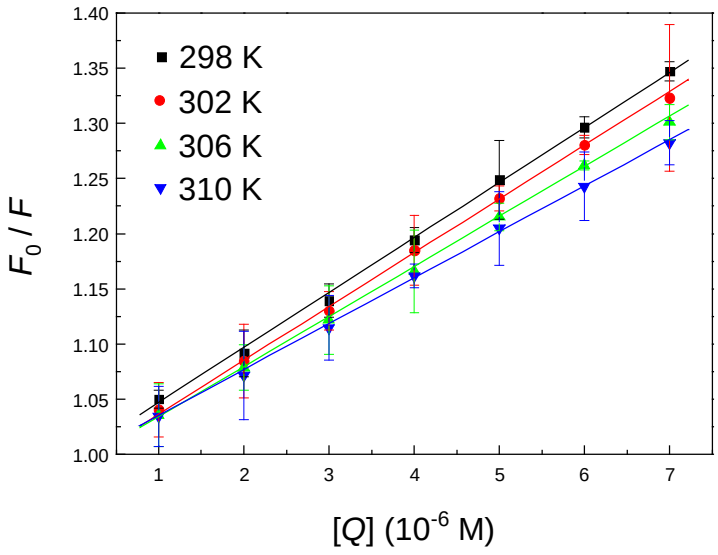

Fig. 4

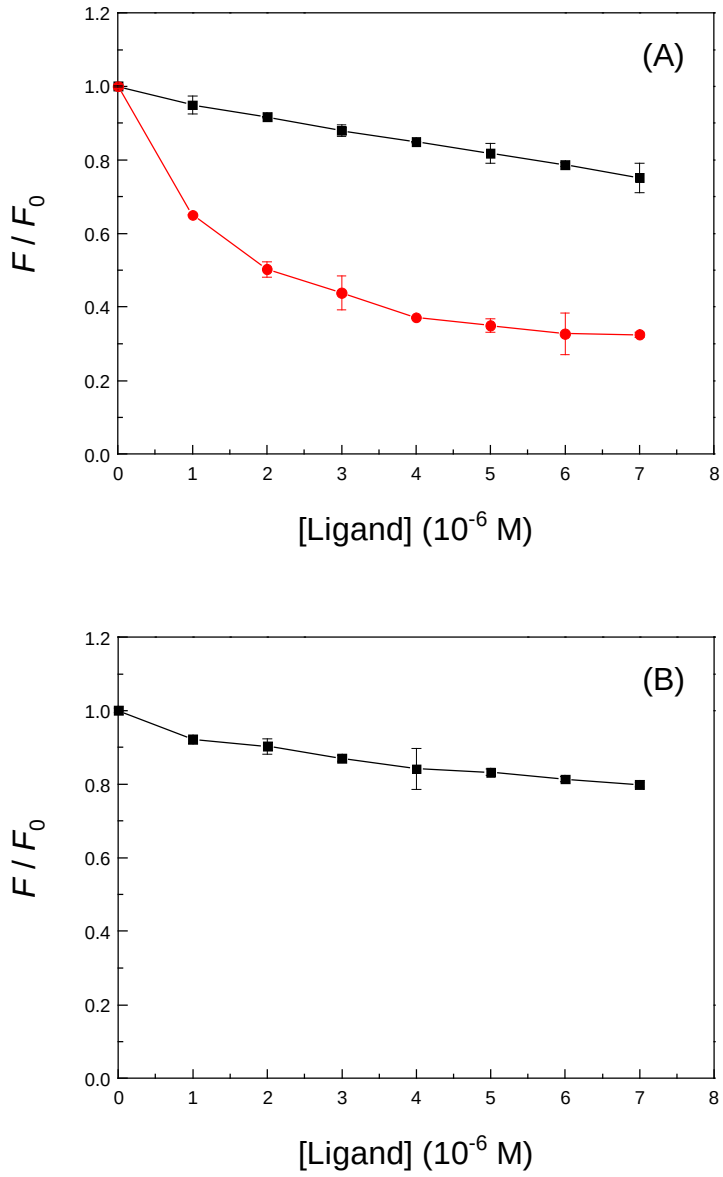

Fig. 5

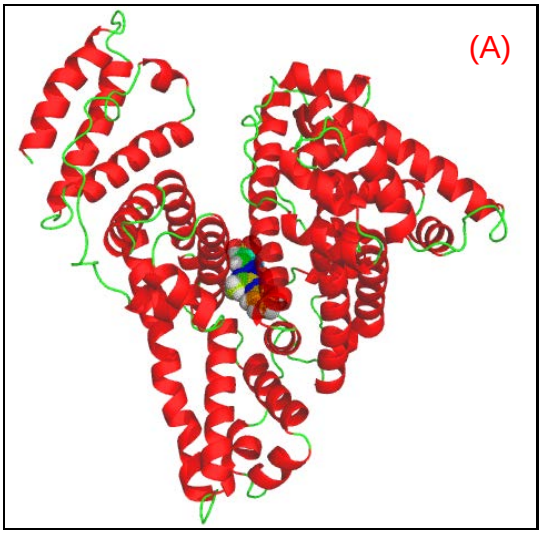

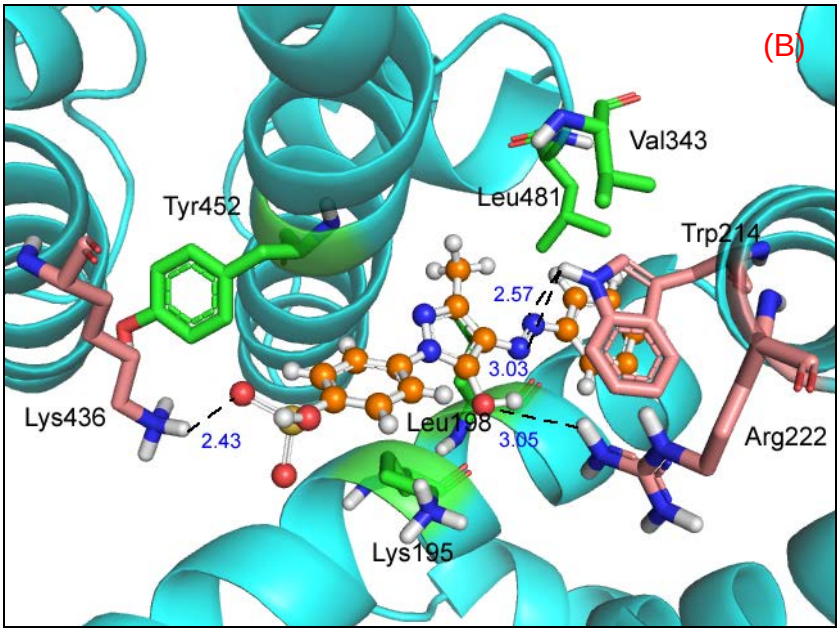

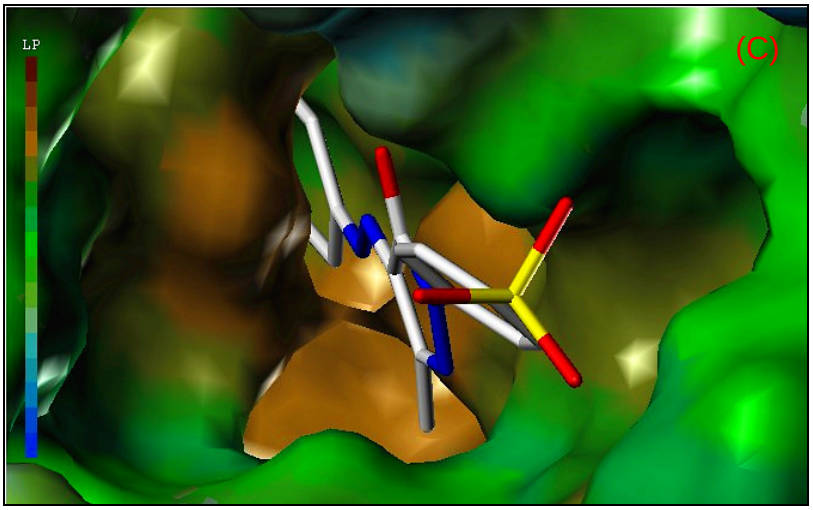

Fig. 6

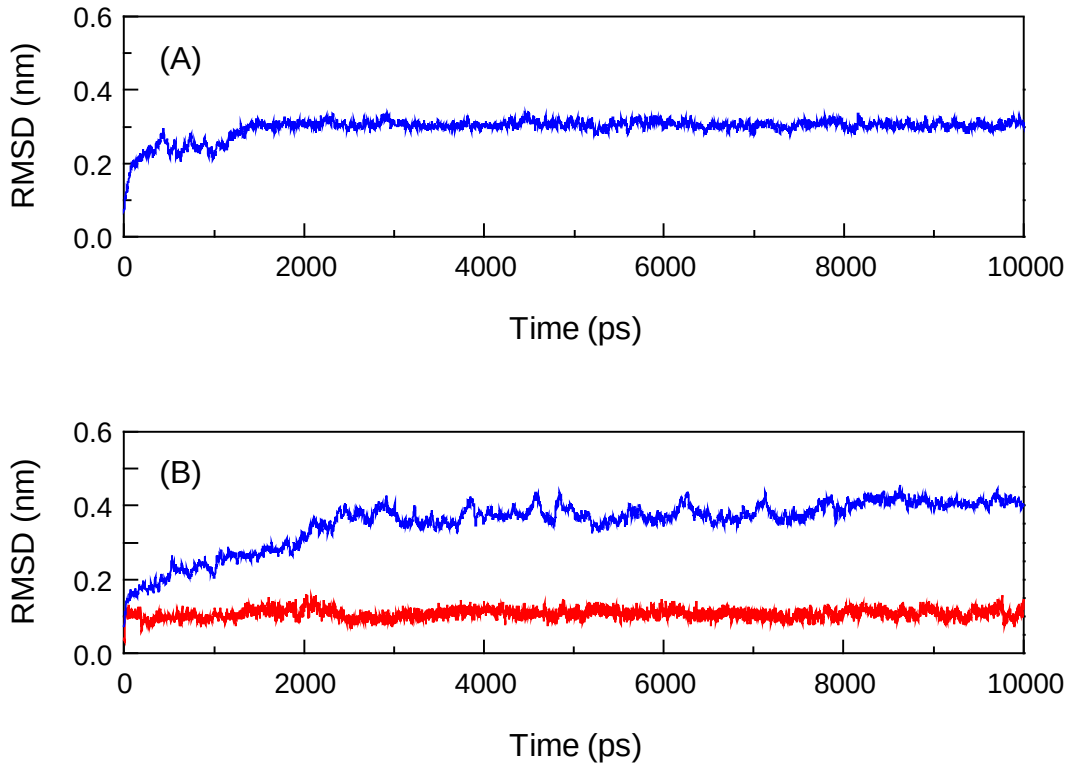

Fig. 7

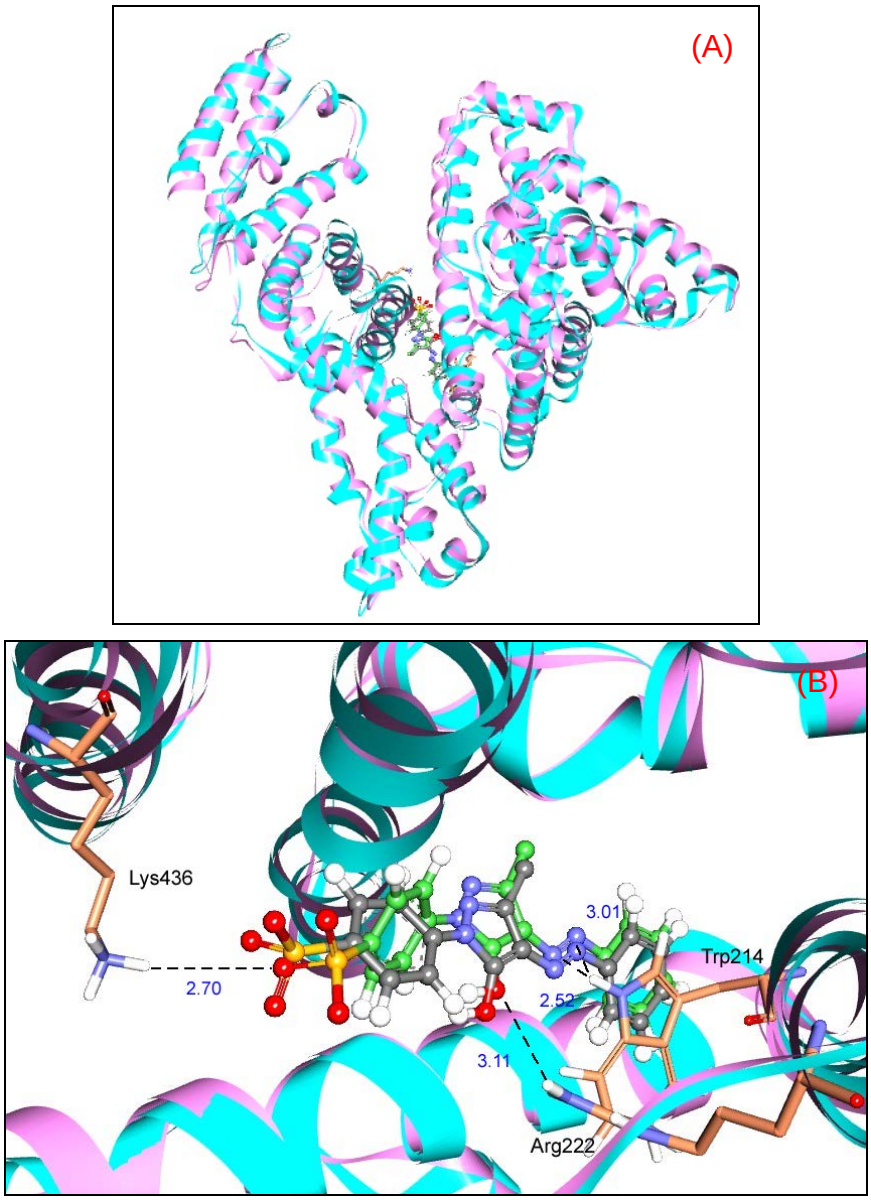

Fig. 8

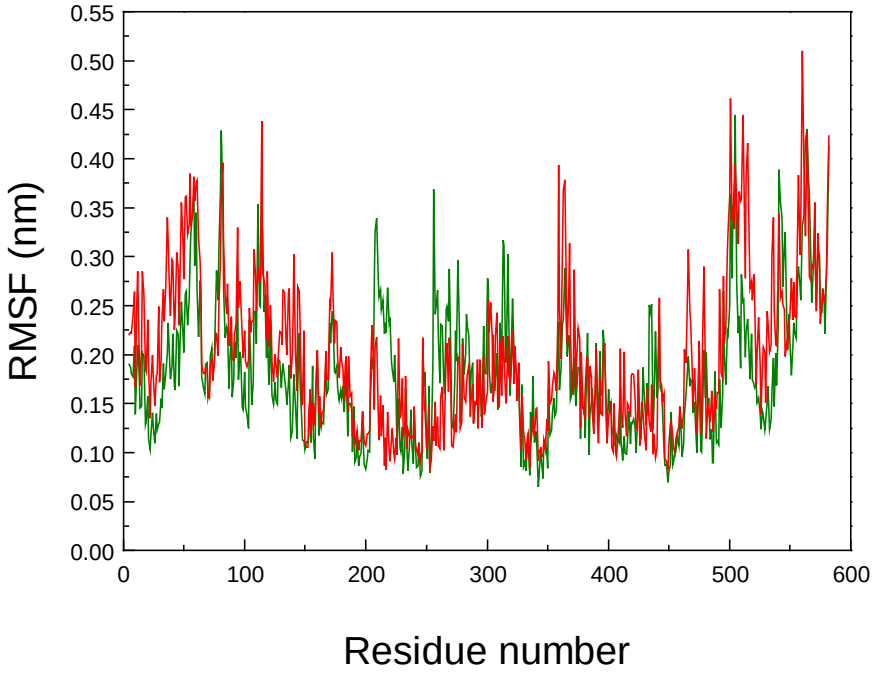

Fig. 9

Supporting Information

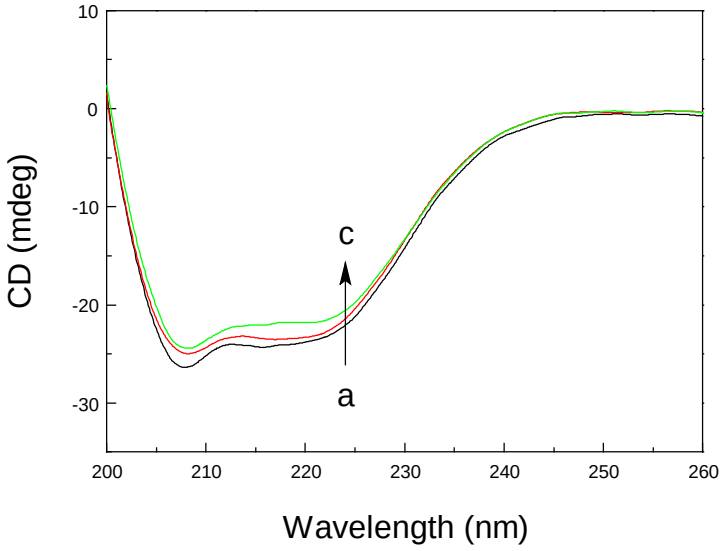

Fig. S1. Far-UV CD spectra of albumin complexes with flavazin (pH＝7.4, T＝298 K). (a) 10 μM albumin; (b) 10 μM albumin＋10 μM flavazin; (c) 10 μM albumin＋20 μM flavazin.

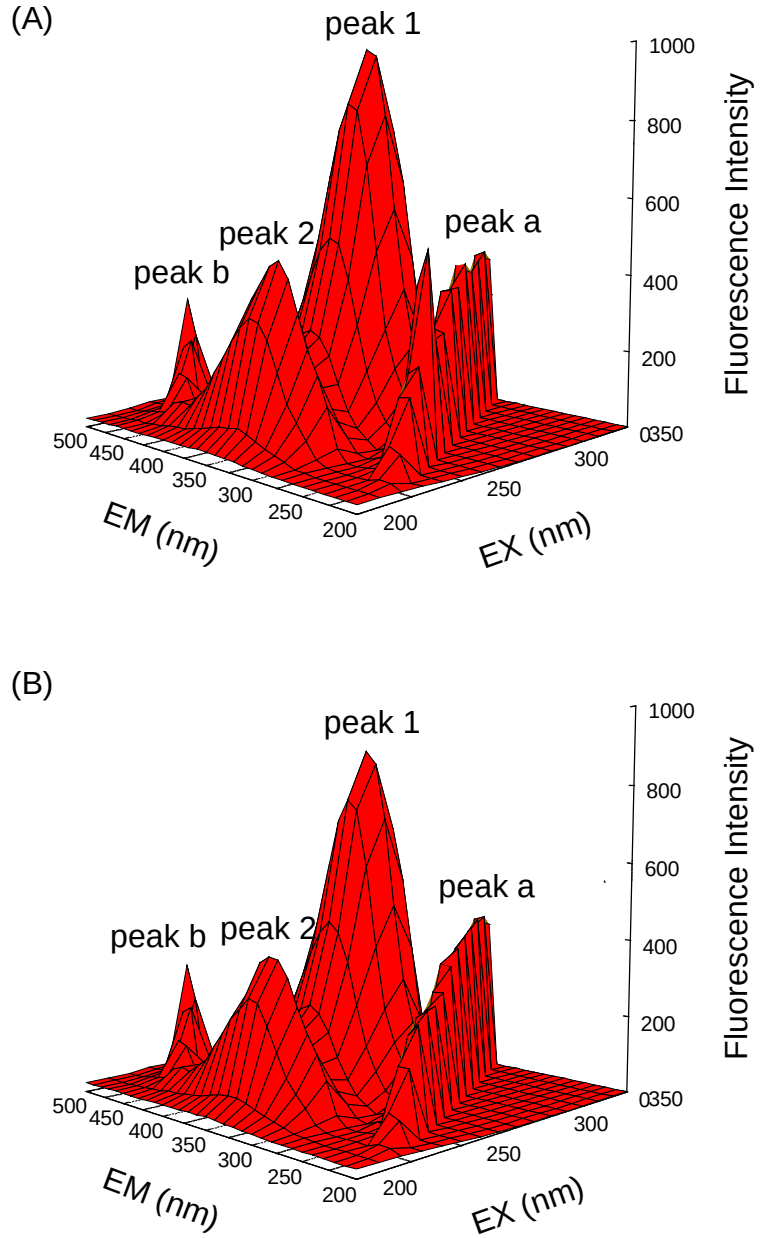

Fig. S2. Three-dimensional fluorescence of albumin (A) and the albumin-flavazin (B) system. (A) c(albumin)＝1.0 μM, c(flavazin)＝0; (B) c(albumin)＝1.0 μM, c(flavazin) ＝1.0 μM; pH＝7.4, T＝298 K.

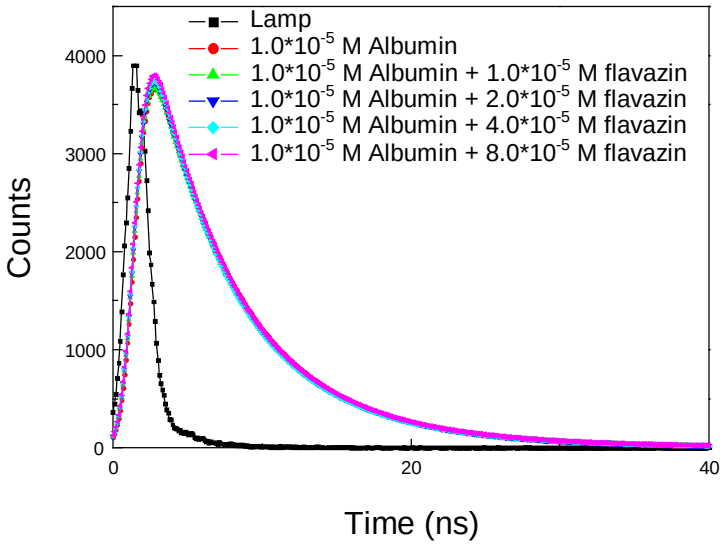

Fig. S3. Time-resolved fluorescence decays of albumin in Tris-HCl buffer (pH＝7.4) as a function of flavazin concentrations. *c*(albumin)＝10 μM, *c*(flavazin)＝0 (red), 10 (green), 20 (blue), 40 (cyan) and 80 (magenta) μM. The sharp pattern on the left (black) is the lamp profile.

Graphic for Table of Contents

The biological activities of azo colorant may significantly be influenced by the biointeraction of ligand to protein in the human body.